Pedestrian Head and Body Pose Estimation with CNN in the Context of Automated Driving

Michaela Steinhoff[1], Daniel Göhring[2]
[1]*Business Area Intelligent Driving Functions, IAV GmbH, Rockwellstr. 3, 38518 Gifhorn, Germany*
[2]*Institute of Computer Science, Freie Universität Berlin, Arnimallee 7, 14195 Berlin, Germany*
michaela.steinhoff@iav.de, daniel.goehring@fu-berlin.de

Keywords: Automated Driving, Convolutional Neural Network, Headpose, Pedestrian Intention, Semi-Supervision

Abstract: The challenge of determining pedestrians head poses in camera images is a topic that has already been researched extensively. With the ever-increasing level of automation in the field of Advanced Driver Assistance Systems, a robust head orientation detection is becoming more and more important for pedestrian safety. The fact that this topic is still relevant, however, indicates the complexity of this task. Recently, trained classifiers for discretized head poses have recorded the best results. But large databases, which are essential for an appropriate training of neural networks meeting the special requirements of automatic driving, can hardly be found. Therefore, this paper presents a framework with which reference measurements of head and upper body poses for the generation of training data can be carried out. This data is used to train a convolutional neural network for classifying head and upper body poses. The result is extended in a semi-supervised manner which optimizes and generalizes the detector, so that it is applicable to the prediction of pedestrian intention.

1 INTRODUCTION

The research on automated driving is more relevant than ever. Semi-automated functions such as automatic parking or driving in stop-and-go traffic have long been available in the form of assistance systems (parking and traffic jam assistant). Even fully automated driving is no longer limited to motorway scenarios. Many projects, like Stimulate[1] in Berlin, master the challenges of urban traffic already completely autonomous, although limited in speed. This work is part of a project, which is contributing to the ongoing development of self-driving cars.

One of the biggest challenges in urban scenarios is the robust prediction of pedestrians. Simple tracking and adapted motion models are not sufficient to map the highly dynamic behaviour of humans. Therefore, countless research groups try to extract more information from the human posture. In addition to a more precise analysis of the leg positions, many researchers also focus on the head pose. Kloeden et al. (2014) have already shown that the head pose is suitable as a characteristic for predicting the movements of pedestrians. They proved that pedestrians show a protection behaviour particularly before crossing the road, which can be attached to the increased head movement. For many decades, classical machine learning has been used to extract this orientation of the head. A common methodology is the quantification of the angular ranges, and thus the declaration of a classification problem (Schulz and Stiefelhagen, 2012). In that work, the authors scan the upper part of a pedestrian image, assuming the head to be there. Eight classifiers are used to locate the head within this part and estimate an initial pose. These classifiers are trained for eight different head pose classes, each with a range of 45°. For the continuous estimation of poses, regression is the preferred method. Lee et al. (2015) and Chen et al. (2016) extract gradient based characteristics like HOG (Histogram of Oriented Gradients) features and then use a SVR (Support Vector Regressor) to estimate the head pose.

All these methods only consider the yaw angle of the head. Contrary to this, the approaches of Rehder et al. (2014), Chen et al. (2011) and Fanelli et al. (2011) take additional orientation directions into account. The latter receives 3D data from a depth camera and uses it to find the position of the tip of the nose as well as the yaw, pitch and roll angles of the head using a Random Regression Forest. A disadvantage of this method is therefore that only a limited area of the possible head poses, namely the one with a visible

[1]https://www.wir-fahren-zukunft.de

nose, can be determined. It is furthermore assumed that the head was detected in the image in advance. Conversely, in Reh-der et al. (2014) monocular RGB images serve as input data, which do not have to be restricted to the head section, but can contain complete as well as covered pedestrians. The head localization is done within the algorithm via HOG/SVM and a part-based detector proposed by Felzenszwalb et al. (2010). Proceeding from this, four discrete classes are defined for the pose estimation, for each of which a classifier is trained using logistic regression with LBP (Local Binary Pattern) features. By integrating the discrete orientation estimates using a HMM (Hidden Markov Model), they obtain continuous head poses. This approach is particularly interesting in that the head poses are plausibilized and impossible poses are discarded with the help of the upper body pose and the motion direction. Chen et al. (2011) go one step further and estimate both the head and body poses in pedestrian images. Therefore, the orientation of the body is divided into eight discrete direction classes and multi-level HOG features are extracted. Furthermore, the yaw angle range of the head is divided into twelve classes and the pitch angle range of the head into three classes. After localizing the head, texture and color features are extracted by another multi-level HOG descriptor and histogram-based color detector. A particle filter framework is subsequently used to estimate the body and head poses. The dependency between the poses as well as the temporal relationship are taken into account. Another approach also estimates both the head and body pose (Flohr et al., 2015). For both poses, eight orientation-specific detectors are trained, whose class centers are shifted by 45° each. To locate the exact body and head position in the image, they make use of disparity information obtained from the stereo input data. Based on this, a DBN (Dynamic Bayesian Network) is used to get the current orientation states. Thereby the current head pose depends on the previous head pose and also on the current body pose.

Recently, (deep) neural networks have become increasingly important and their application also aims for an improvement of the head pose detection. Latest nets as presented in (Patacchiola and Cangelosi, 2017) or (Ruiz et al., 2017) predict yaw, pitch and roll angles in a continuously manner and achieve great accuracy. The input, however, is also here only the head section, which must be available in relatively high resolution. If these approaches are to be used in the context of automatic driving, pedestrians and their head positions must be recognized early, i.e., from a great distance, so that the poor quality of the input data does not fulfill the requirements of the mentioned methods. The present work, therefore, presents a neural network that recognizes head poses from images with the quality of cameras commonly used in vehicles. Not only the head but the entire pedestrian's image section serves as input, since the head pose in relation to the upper body provides further important information. From this it can be deduced, for example, whether a pedestrian shows a safety behaviour, which is a clear indication of the intention to cross the road. For the training of this head and upper body pose detector, commonly available data sets for head poses and pedestrians in general like Human3.6m[2], PETA[3] or INRIA[4] cannot be used, because the reference to the upper body alignment is missing. In addition, most researchers only consider yaw angles in the range of -90° to 90°, i.e., the frontal view of the pedestrian heads. In the present project, however, it is just as important whether a passer-by perceives oncoming traffic or the automated driving vehicle. Therefore, a framework for the generation of a "full-range" data set will be briefly presented here. Using a semi-supervised approach, a trained convolutional neural network (CNN) is extended so that the comparatively small amount of self-generated annotated data is enriched by many unlabeled data from real test drives within the project and the detector achieves more accurate results.

The contributions of this work can be summarized in the following key points:

- a framework for generating a data set with head and upper body poses,
- training and evaluation of a network (CNN) using the data set,
- enhancement of training data with real driving data,
- evaluation of an approach to semi-supervised learning and improvement of the network.

The paper is structured as follows:

After the second chapter presented the framework for data set generation, Chapter 3 gives a detailed description of our detector design. The obtained results are illustrated in the following chapter. Chapter 5 draws a conclusion and presents an outlook for future work.

[2]http://vision.imar.ro/human3.6m/description.php
[3]http://mmlab.ie.cuhk.edu.hk/projects/PETA.html
[4]http://pascal.inrialpes.fr/data/human

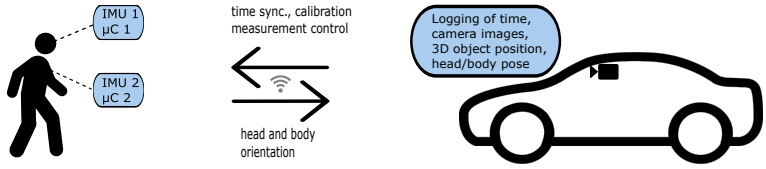

Figure 1: The used framework setup for data set generation.

2 DATA SET GENERATION

As already mentioned, this work requires data that is not annotated in the common pedestrian data sets. The added value lies in the fact that not only the pose of the head, but also that of the upper body in relation to the head is considered. In order to annotate such data automatically, a data generation setup and software framework was developed which can be applied to capture images of pedestrians together with the corresponding head and upper body poses. Therefore this section first explains the experimental setup and the processing infrastructure after that. An overview of the framework setup is given in Figure 1.

2.1 Experimental Environment

The images were taken by a camera installed in a test vehicle alongside other sensors such as Lidar. The vehicle was also equipped with an object tracking module, which outputs 3D positions of the pedestrians in vehicle coordinates. Two inertial sensors (MPU6050) with 6 degrees of freedom each were used to measure the exact head and upper body orientations. Together with one microcontroller with integrated WiFi module (ESP8266 – 12F) each, these were placed on the head and upper body of the test persons. Since the position and orientation of the MPU6050s on the head and body depend a lot on the probands and the upcoming measurement, an online calibration was performed at the beginning of each exposure and the sensor values were transformed into quaternions relative to the corresponding initial pose. In addition, IMU (inertial measurement unit) drift compensation was carried out beforehand and the drift behavior was analyzed in the following. With an average duration of the measurement sequences of 2 minutes, the drift of 0.5° per minute was negligible.

2.2 Processing Infrastructure

The control of the IMU, the online calibration and the time synchronization via ntp server were realized in Arduino on the microcontrollers. The measured poses and the related timestamps were sent via TCP to a logging computer where they were processed and added to the data set. A single date then consists of the timestamp with corresponding image, the 3D object position and yaw, pitch and roll angles of either head and the upper body. A total of 2500 test and training data was annotated, including recordings of 20 different people at different times of the day and year.

3 HEAD AND UPPER BODY POSE DETECTOR

This section introduces the developed head pose detector. First of all, the definition of the individual classes is discussed. The training process is divided into the two parts supervised and its unsupervised extension, which are explained in the following two subchapters.

3.1 Class Definition

The detector presented in this paper is intended to detect the yaw angles of the head and upper body. Since we want to address a classification problem, the annotated data has to be mapped to classes. Therefore, the possible head poses in the range $[-105^\circ, 105^\circ]$ are quantized in $\alpha_H = 30^\circ$ steps, whereby a yaw angle of 0° implies the head pointing directly towards the camera. All following angles are specified in this definition of coordinate system.

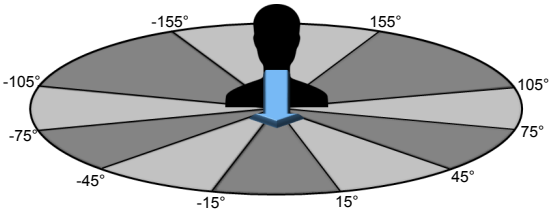

Figure 2: The head pose range is divided into 10 classes.

The range $]105°,180°] \cup [-180°,-105°[$ (i.e., facing away from the camera) is divided into three parts á $\alpha_{H2} = 50°$. Accordingly there are $n_{hc} = 10$ head classes in total (see Figure 2). For anatomical reasons, the deviation of the upper body pose from the head pose is limited to a range of $-90°$ to $+90°$. This area is divided into $n_{bc} = 3$ body classes C_B depending on the head pose. The body either points left ($C_B = 0$), right ($C_B = 2$) or in the same direction as the head ($C_B = 1$). This results in an overall number of 30 classes for the detector. The output class C_{out} resulting from the head (C_H) and upper body (C_B) class is calculated according to Eq. 1. The head and upper body class are derived from the respective yaw angles ψ_H and ψ_B.

$$C_{out} = C_B \cdot n_{hc} + C_H \tag{1}$$

with

$$C_H = \begin{cases} \lfloor \frac{\psi_H - \frac{1}{2}\alpha_H}{\alpha_H} \rceil + \frac{n_{hc}}{2} & , \text{if } -105° \leq \psi_H \leq \frac{\alpha_H}{2} \\ \lfloor \frac{\psi_H - \frac{1}{2}\alpha_H}{\alpha_H} \rceil + \frac{n_{hc}}{2} + 1 & , \text{if } \frac{\alpha_H}{2} < \psi_H \leq 105° \\ \lfloor \frac{\psi_H - \frac{1}{2}\alpha_{H2}}{\alpha_{H2}} \rceil + \frac{n_{hc}}{2} - 1 & , \text{if } \psi_H < -105° \\ \lfloor \frac{\psi_H - \frac{1}{2}\alpha_{H2}}{\alpha_{H2}} \rceil + \frac{n_{hc}}{2} + 1 & , \text{if } 105° < \psi_H \leq 155° \\ 0 & , \text{otherwise} \end{cases} \tag{2}$$

and

$$C_B = \lfloor \frac{\delta\psi}{\alpha_B} + \frac{1}{2} \rceil + \lfloor \frac{n_{bc}}{2} \rceil \tag{3}$$

where

$$\delta\psi = \begin{cases} \psi_H - \psi_B + 360° & , \text{if } \psi_H - \psi_B < -180° \\ \psi_H - \psi_B - 360° & , \text{if } \psi_H - \psi_B > +180° \\ \psi_H - \psi_B & , \text{otherwise} \end{cases} \tag{4}$$

3.2 Semi-Supervised Learning with CNN

In the domain of neural networks, CNN have been established to handle classification tasks. Most of the best-known classification networks are trained in a supervised manner with a large amount of annotated data. Since the present use case makes different demands on the annotation, only the few self-generated data are available in comparison. The idea to train a reliable classification network from it nevertheless is based on a semi-supervised approach.

Figure 3: Samples of unlabeled data, the first row shows unsorted, the second and third row clustered samples.

Supervised Learning

As mentioned above, CNN are very well suited to solving classification problems and there are many proven network architectures. Hence, a CNN is also used here and the layer topology is oriented to these architectures. Figure 4 shows a schematic representation of the underlying network structure.

The input data is scaled to a fixed size (128*x*128) and converted to grayscale values. They subsequently pass through three consecutive blocks each with three convolutional and one maxpooling layer until a fully connected layer maps them to an embedding vector with size 64, which is transformed to logit class scores by a final dense layer. During training, a dropout layer located between the last two fully-connected layers was used with a dropout rate of 0.5 in order to generalize the learning result. To find the best hyper parameters for the training, a grid search was applied. Accordingly, the following parameter configuration provides the best performance and has been used further:

Table 1: Best parameters found by grid search.

batchsize	50
initial learning rate	0.0001
learning rate decay	0.33
decay steps	10000
optimizer	Adam
loss function	Cross Entropy

The loss function of the supervised part with labels λ and predicted outputs y is given by

$$loss_{logit} = -\sum_x \lambda \cdot \log(y + 1e^{-8}). \tag{5}$$

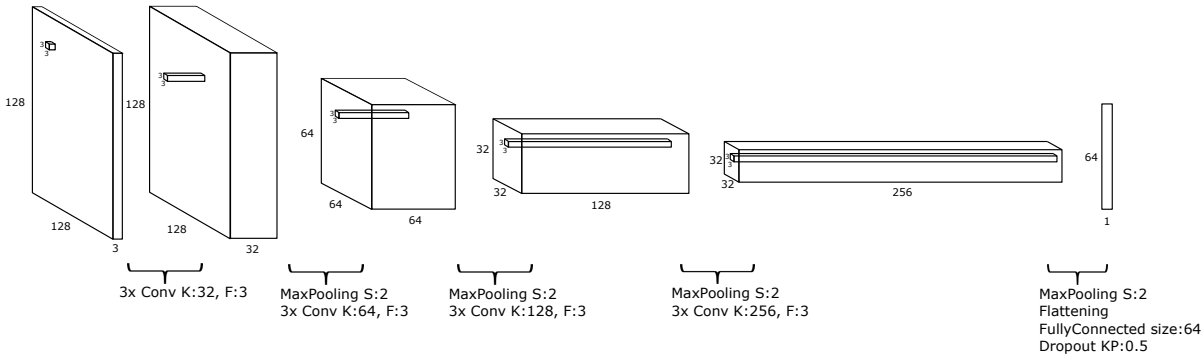

Figure 4: Schematic representation of the used network architecture.

Semi-Supervised Extension

Due to the comparably small variance of the training data, the network performed well on similar testing data. With the aim of optimizing and generalizing the network, it was extended to include unsupervised learning. In general, as with most semi-supervised methods, the results of supervised learning are improved by clustering the unlabeled data and then assigning them to already trained classes. Inspired by the concept of Haeusser et al. (2017), the assignment is not based on the last but the penultimate layer. In this so-called "embedding" level, the similarity of all unlabeled data to the labeled data is determined. An actual assignment of the unlabeled data only takes place if it has been attributed to the same class label twice due to the highest similarity. To find a suitable scale for this similarity, different metrics were tested and compared to each other. The following two metrics have emerged as the ones with the best-performing results.

The *cosine similarity* describes the correspondence of the orientations of two vectors to be compared. For this purpose the cosine of the angle between them is determined according to Eq. 6.

$$\cos(\theta) = \frac{a \cdot b}{\|a\| \, \|b\|} \tag{6}$$

The resulting value range for this scale is therefore limited to [-1, 1], where '1' means that the orientation of both vectors is identical ($\theta = 0°$). '-1' however denotes an opposite orientation ($\theta = 180°$) and '0' signifies the vectors are orthogonal to each other ($\theta = 90°$). Aside from being independent of the vectors magnitudes, this metric has the advantage that it is very computation-performant, since only the dot product has to be calculated. The loss is determined analogue to Haeusser et al. (2017) by comparing the resulting association probability with the expected probability distribution using cross entropy.

The *Mahalanobis distance* indicates the distance of a data point to the mean of a point distribution of one class in multiples of the standard deviation. Thus, in contrast to the *Euclidean distance*, the correlation between the data points is taken into account and the assignment to individual clusters of data (classes) becomes more accurate.

If $\vec{x}$ is a data point to be assigned and $\vec{\mu}$ is the mean value of the data set of a class with covariance matrix C, the Mahalanobis distance is given by:

$$D_M(\vec{x}) = \sqrt{(\vec{x}-\vec{\mu})^T C^{-1} (\vec{x}-\vec{\mu})} \tag{7}$$

The result initially expresses the dissimilarity of the sample to the data set. By scaling to the value range $D_{Ms} = [0,1]$, reverting the range and normalizing the multiplication of this association probability with its transposed the following probability distribution is obtained stating that several unlabeled data points are associated with the respective classes:

$$p = ||(p_A \cdot p_A^T)||_2 \tag{8}$$

with

$$p_A = 1 - D_{Ms} \tag{9}$$

The expected probability distribution p_E in this case is equal to the unit matrix with rank n_C (number of classes), since a sample is to be assigned uniquely to one class. For this purpose it must be ensured that each class is represented with at least one sample per batch in the set of unlabeled data. This is achieved by adding one labeled sample for each class to the batch with unlabeled samples. The total loss is finally calculated by applying cross entropy on these probabilities and adding the result to the logit loss from the supervised part (see Eq.5).

$$loss = -\sum_x p_E \cdot \log(p_A + 1e^{-8}) + loss_{logit} \tag{10}$$

Table 2: Train error, test error, average precision (AP), average recall (AR) and test error including 'adjacent classes' (TE*) of SUP, COS and MAHA in [%]. The last two columns declare the distribution of train and test samples within the supervised and the semi-supervised methods.

	train err	test err	AP	AR	TE*	train samples	test samples
SUP	0.17	82.19	16.96	18.27	54.86	2000	500
COS	30.59	66.55	32.57	25.17	43.52	12000	500
MAHA	0.41	58.53	32.26	30.21	32.15	12000	500

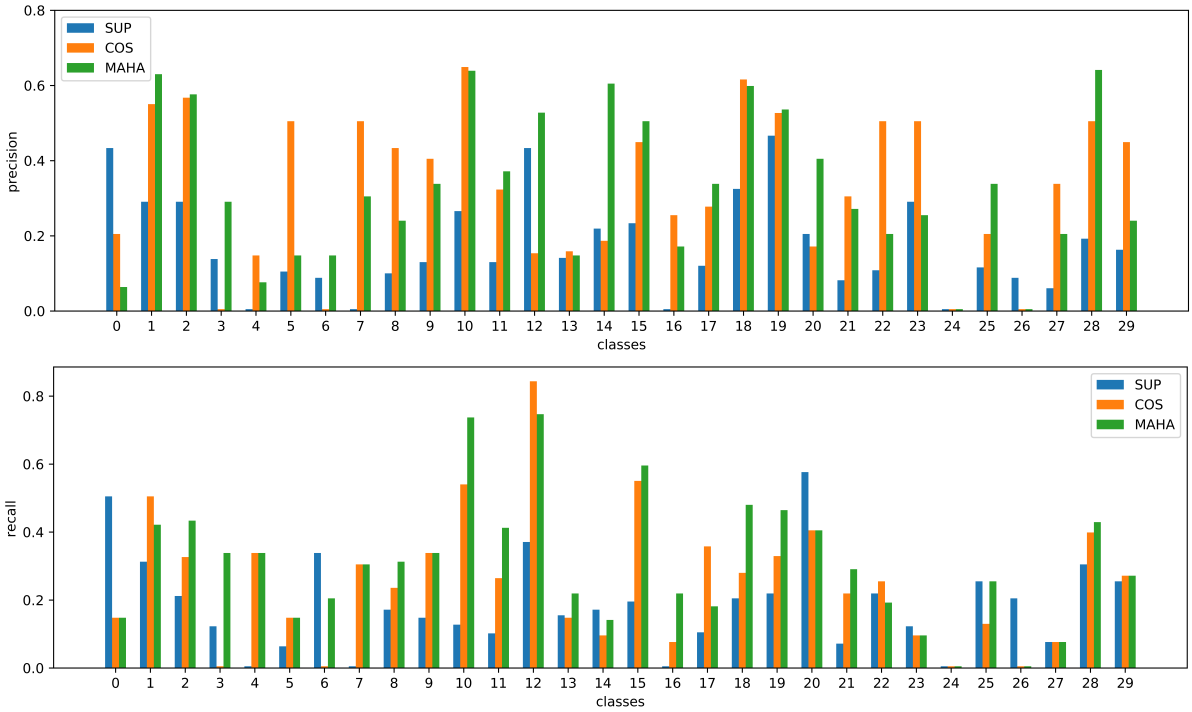

Figure 5: Precision and recall of the trained networks, the results of the semi-supervised approaches (COS and MAHA) improve the supervised one (SUP).

4 EXPERIMENTS

For the training of the head pose detector 2500 labeled and 10000 unlabeled data were used. It was performed on a computer with four GTX 2080 Ti with 12 GB memory each. Because of the high imbalance of the class distribution in the labeled training data set, the maximum number of samples used per class in all three trainings was limited to avoid overfitting of more frequent classes. This was already recommended by Weiss and Provost (2001), who showed that an unequal distribution does not usually lead to the best performance. In the following, the results of the purely supervised trained network (further referred to as SUP) and the two different methods for estimating similarity within the semi-supervised trained network (MAHA for the one using the mahalanobis distance, COS for the cosine similarity) are compared. Due to the small number of labeled samples, SUP converged comparatively quickly after about 500 epochs. With the best parameters found by the grid search, a training error of 0.17% was achieved. But the evaluation with test data confirmed that the network specialized in the training data. The error rate for the randomly distributed test data was 82.19% at best (see Table 2).

In the approach of association using cosine similarity, it was necessary that each class is represented in each batch of labeled data so that each unlabeled sample can be assigned properly as well. Depending on the number of samples used per class per batch, this results in very large batch sizes for 30 classes, which caused memory issues. But with 10 samples per class per batch a suitable compromise between training efficiency and executability was found. This of course led to a declining of the obtained network accuracy, resulting in a training error of about 30%. Nevertheless, this as well as the second semi-supervised

solution MAHA reduces the test error by a relevant amount, which is also reflected in Figure 5, depicting the precision and recall per class of all three approaches. Even if individual classes perform worse for COS and MAHA than for SUP, the average precision (AP) and recall (AR) noticeably are higher as can be seen in Table 2. And although MAHA also required restrictions in parameter selection due to the limited memory capacity, this approach yielded the lowest test error of 59.17%. The fact that the semi-supervised approaches generalize the training result and thus enhance it is particularly evident when the confusion matrix is analyzed more closely. Therefore Figure 6 illustrates the confusion matrix of MAHA. For comparison, those of SUP and COS can be found in the appendix. First of all, it is conspicuous that test samples of other classes are assigned more often to the columns 10 to 19, which correspond to the classes with the same alignment of head and upper body. This is probably due to the fact that this natural human pose occurs more frequently in the unlabeled data set and thus their training was more effective. Furthermore, the principal diagonal is highlighted in dark blue as these cells map the amount of true positives. According to the class definition in Section 3, the classes ending with the same number (e.g. 3, 13 and 23) represent the same head class. These cells are also shaded light blue. The remaining cells are marked darker gray the higher their cell value is. Mainly in contrast to the confusion matrix of SUP (see Figure 8), whose predictions are highly scattered, an orientation of the predicted classes to the principal diagonal as well as partially to the secondary diagonals of the same head classes can be observed here.

	0	1	2	3	4	5	6	7	8	9	10	11	12	13	14	15	16	17	18	19	20	21	22	23	24	25	26	27	28	29
0	14	42	0	0	0	0	0	0	0	14	0	14	0	0	0	14	0	0	0	0	0	0	0	0	0	0	0	0	0	0
1	7	53	0	0	0	0	0	0	0	0	0	30	0	0	0	0	0	7	0	0	0	0	0	0	0	0	0	0	0	0
2	0	5	33	11	0	0	0	0	0	0	0	5	5	0	22	5	5	0	0	0	0	0	0	5	0	0	0	0	0	0
3	0	0	9	36	0	0	0	0	0	0	0	9	0	27	0	0	0	0	0	0	9	0	0	0	0	0	0	9	0	0
4	0	0	0	0	0	25	0	0	0	0	0	0	0	25	25	0	0	0	0	0	0	0	0	0	0	0	0	0	0	25
5	16	0	0	16	16	16	0	0	0	0	0	0	0	0	0	0	16	0	0	0	0	0	0	0	0	0	0	0	0	0
6	0	0	0	0	0	0	66	0	0	0	33	0	0	0	0	0	0	0	0	0	0	0	0	0	0	0	0	0	0	0
7	0	0	0	0	20	0	20	20	0	0	0	0	0	0	0	0	0	0	40	0	0	0	0	0	0	0	0	0	0	0
8	0	0	0	0	0	0	0	0	33	33	0	0	0	0	0	11	0	11	0	0	0	0	0	0	0	0	0	0	11	0
9	0	0	0	20	0	0	0	0	0	40	20	0	0	0	0	0	0	0	0	0	0	0	0	0	0	0	0	0	20	0
10	0	0	2	0	0	0	0	0	2	2	67	1	1	0	0	5	0	1	7	0	1	2	0	0	1	0	0	1	0	0
11	10	0	0	0	0	0	0	0	3	0	13	41	10	6	0	0	3	0	0	0	0	3	6	0	0	0	0	0	0	0
12	3	9	0	0	0	0	0	0	0	0	0	9	46	12	3	0	0	0	6	0	0	0	0	0	3	3	3	0	0	0
13	0	0	6	0	0	0	0	0	0	0	0	0	12	31	18	0	0	0	6	0	0	0	0	6	0	0	0	0	12	6
14	0	0	7	7	0	0	0	0	0	7	0	7	7	23	7	15	0	0	0	0	0	0	0	7	0	0	7	0	0	0
15	0	0	13	3	0	0	0	0	0	0	6	6	0	0	0	50	3	0	0	6	0	0	0	0	0	0	0	6	3	0
16	0	0	0	0	0	0	0	0	0	0	0	0	8	0	8	8	16	33	8	8	0	0	0	0	0	0	0	0	0	8
17	0	0	0	9	0	0	0	0	0	0	0	0	0	0	0	18	27	36	0	0	0	0	0	0	0	0	0	0	9	0
18	0	0	0	0	0	5	2	0	2	0	0	0	11	0	0	2	2	0	61	5	0	0	0	0	0	0	0	2	2	
19	0	0	0	0	0	0	0	3	3	0	11	7	3	3	0	0	0	0	7	42	3	3	0	0	0	0	0	0	0	7
20	0	0	0	0	0	0	0	20	0	10	10	0	0	0	0	10	0	0	10	30	10	0	0	0	0	0	0	0	0	0
21	10	0	10	0	0	0	0	0	0	0	20	0	0	0	0	0	0	0	0	20	0	30	10	0	0	0	0	0	0	0
22	0	0	0	0	0	0	0	0	0	0	0	33	33	0	0	0	0	0	0	0	0	0	16	0	0	16	0	0	0	0
23	0	0	25	0	0	0	0	0	0	0	0	0	0	0	0	0	0	0	0	0	0	0	0	50	25	0	0	0	0	0
24	20	0	0	0	0	0	0	0	0	0	0	0	0	0	20	0	0	0	0	0	0	0	20	20	20	0	0	0	0	0
25	14	0	0	0	0	0	0	0	0	0	0	0	14	14	0	14	0	0	0	0	0	0	0	14	0	14	14	0	0	0
26	0	0	0	0	0	0	0	0	0	0	0	0	0	25	0	0	0	0	0	0	0	0	0	0	0	0	25	25	0	25
27	0	0	0	0	0	0	0	0	7	0	0	0	0	23	7	23	7	0	7	0	0	0	0	0	0	0	15	0	7	0
28	0	0	7	0	3	0	0	0	0	0	3	0	0	0	0	11	3	3	7	0	0	0	0	0	0	0	0	3	53	0
29	0	0	0	0	0	0	0	10	0	0	0	0	10	0	0	0	0	0	20	20	20	0	0	0	0	0	0	0	0	20

Figure 6: Confusion matrix of MAHA, rows index the predicted and columns the actual classes.

In addition, cells of *adjacent classes*, i.e., those which differ only in the head pose by a maximum of 30°, were colored green. It becomes plausible that a high percentage of test samples are associated with these cells regarding the fact that these small differences are difficult to detect, as can be seen in Figure 7. Considering this in the error calculation and including the *adjacent classes* in the set of correct predictions, results in the test error listed in Table 2 under TE*, which for MAHA is only 32.15%.

Figure 7: Prediction example, Left: a sample incorrectly predicted as class 14, Right: an actual sample of class 14.

5 CONCLUSIONS

In this paper, a head pose detector was presented that meets the special requirements of automated driving. Since the relative pose of the upper body was of importance in the project within which the work was developed, in addition to the pure yaw angle of the head, a new data set was generated. Conceived for this purpose, a reference data measuring setup with software framework was used to generate data for training and evaluating a neural network. Due to the relatively small amount of data, the performance of this purely supervised trained classifier was, as expected, poorly. Therefore, the data set was enriched by the numerous unlabeled data available from test drives in the project and an approach of semi-supervised learning was developed and optimized. The test result was thus improved by almost 25%. Furthermore, it was found that many of the misclassifications were associated with the so-called *adjacent classes*. In the context of automated driving, one of the strongest motivations for the detection of head poses is the assessment of whether a pedestrian has perceived the driving vehicle or not. It could be demonstrated that the small pose differences between two adjacent classes are often very difficult to identify and have little influence on the determination of whether the vehicle was seen or not. An adjusted test error of only about 32% could be reported.

Overall, it was found that the semi-supervised method used is very well suited to improve the performance of the head pose detector despite a small data set. In the future, further result optimizations can be achieved by more labeled training data. In addition, better performance will be obtained by upgrading the computer's performance and memory capacity.

REFERENCES

Chen, C., Heili, A., and Odobez, J. (2011). A joint estimation of head and body orientation cues in surveillance video. In *2011 IEEE International Conference on Computer Vision Workshops (ICCV Workshops)*, pages 860–867.

Chen, J., Wu, J., Richter, K., Konrad, J., and Ishwar, P. (2016). Estimating head pose orientation using extremely low resolution images. In *2016 IEEE Southwest Symposium on Image Analysis and Interpretation (SSIAI)*, number 1, pages 65–68. IEEE.

Fanelli, G., Gall, J., and Van Gool, L. (2011). Real time head pose estimation with random regression forests. In *Computer Vision and Pattern Recognition (CVPR), 2011 IEEE Conference on*, pages 617–624. IEEE.

Felzenszwalb, P. F., Girshick, R. B., McAllester, D., and Ramanan, D. (2010). Object detection with discriminatively trained part-based models. *IEEE Transactions on Pattern Analysis and Machine Intelligence*, 32(9):1627–1645.

Flohr, F., Dumitru-Guzu, M., Kooij, J. F. P., and Gavrila, D. M. (2015). A probabilistic framework for joint pedestrian head and body orientation estimation. *IEEE Transactions on Intelligent Transportation Systems*, 16(4):1872–1882.

Haeusser, P., Mordvintsev, A., and Cremers, D. (2017). Learning by association - a versatile semi-supervised training method for neural networks. In *IEEE Conference on Computer Vision and Pattern Recognition (CVPR)*.

Kloeden, H., Brouwer, N., Ries, S., and Rasshofer, R. (2014). Potenzial der Kopfposenerkennung zur Absichtsvorhersage von Fußgängern im urbanen Verkehr. In *FAS Workshop Fahrerassistenzsysteme, Walting, Germany*.

Lee, D., Yang, M.-H., and Oh, S. (2015). Fast and accurate head pose estimation via random projection forests. In *Proceedings of the IEEE International Conference on Computer Vision*, pages 1958–1966.

Patacchiola, M. and Cangelosi, A. (2017). Head pose estimation in the wild using convolutional neural networks and adaptive gradient methods. *Pattern Recognition*, 71:132 – 143.

Reh-der, E., Kloeden, H., and Stiller, C. (2014). Head detection and orientation estimation for pedestrian safety. In *Intelligent Transportation Systems (ITSC), 2014 IEEE 17th International Conference on*, pages 2292–2297. IEEE.

Ruiz, N., Chong, E., and Rehg, J. M. (2017). Fine-grained head pose estimation without keypoints. *CoRR*, abs/1710.00925.

Schulz, A. and Stiefelhagen, R. (2012). Video-based pedestrian head pose estimation for risk assessment. In *2012 15th International IEEE Conference on Intelligent Transportation Systems*, pages 1771–1776.

Weiss, G. and Provost, F. (2001). The effect of class distribution on classifier learning: An empirical study. Technical report.

6 APPENDIX

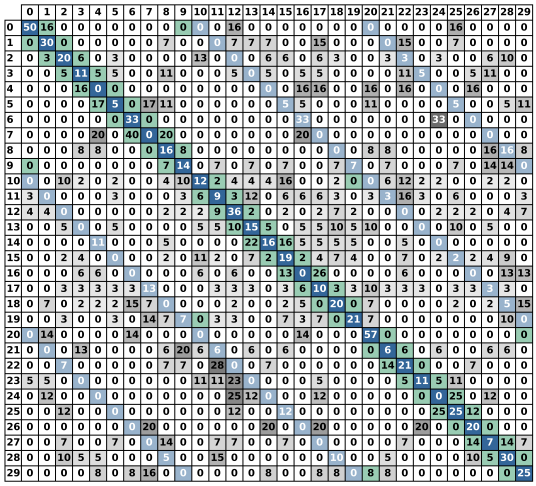

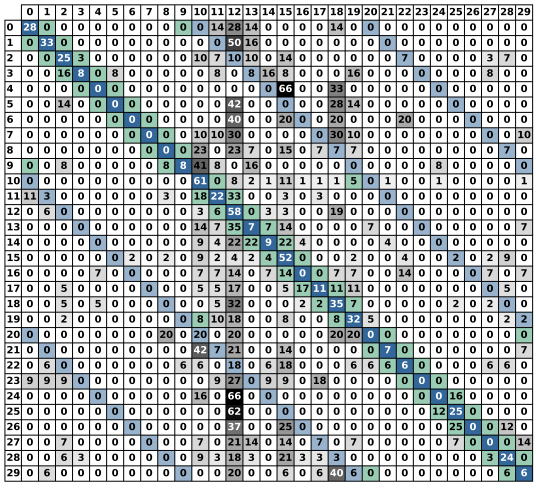

Figure 8: Confusion matrices of the supervised (top) and the cosine (bottom) approach.